LAWRENCE
LIVERMORE
NATIONAL
LABORATORY

LLNL-JRNL-423106

The Role of Radiation Transport in the Thermal Response of Semi-Transparent Materials to Localized Laser Heating

Jeffrey Colvin, Aleksei Shestakov, James Stolken,
Ryan Vignes

February 3, 2010

Journal of Applied Physics

Disclaimer

This document was prepared as an account of work sponsored by an agency of the United States government. Neither the United States government nor Lawrence Livermore National Security, LLC, nor any of their employees makes any warranty, expressed or implied, or assumes any legal liability or responsibility for the accuracy, completeness, or usefulness of any information, apparatus, product, or process disclosed, or represents that its use would not infringe privately owned rights. Reference herein to any specific commercial product, process, or service by trade name, trademark, manufacturer, or otherwise does not necessarily constitute or imply its endorsement, recommendation, or favoring by the United States government or Lawrence Livermore National Security, LLC. The views and opinions of authors expressed herein do not necessarily state or reflect those of the United States government or Lawrence Livermore National Security, LLC, and shall not be used for advertising or product endorsement purposes.

The Role of Radiation Transport in the Thermal Response of Semi-Transparent Materials to Localized Laser Heating

Jeffrey Colvin,* Aleksei Shestakov, James Stölken, and Ryan Vignes

Lawrence Livermore National Laboratory

ABSTRACT

Lasers are widely used to modify the internal structure of semi-transparent materials for a wide variety of applications, including waveguide fabrication and laser glass damage healing. The grey diffusion approximation used in past models to describe radiation cooling is not adequate for these materials, particularly near the heated surface layer. In this paper we describe a new computational model based upon solving the radiation transport equation in 1D by the P_n method with ~500 photon energy bands, and by multi-group radiation diffusion in 2D with fourteen photon energy bands. The model accounts for the temperature-dependent absorption of infrared laser light and subsequent redistribution of the deposited heat by both radiation and conductive transport. We present representative results for fused silica irradiated with 2-12 W for 5-10 s pulse durations in a 1-mm spot, which is small compared to the diameter and thickness of the silica slab. We show that, unlike the case for bulk heating, in localized infrared laser heating radiation transport plays only a very small role in the thermal response of silica.

Keywords: laser processing, radiation transport in glass

*Corresponding author: colvin5@llnl.gov

I. Introduction

Low-power infrared lasers are used to modify the internal structure of semi-transparent materials for a wide variety of applications, including waveguide fabrication [1], texturing of computer discs [2], and laser glass-damage mitigation [3], which is the application with which we are concerned in this study. In the bulk heating of silica, where depth and/or extent of the heated region is comparable in size to the material thickness or width, such as in optical fiber manufacture, there has been a long-standing recognition that radiation transport can play an important role in the overall heat flow history in the material [4]. Tian and Chiu have presented heat flow models for thin glass rods that include radiation transport [5,6]. Heating of thin glass rods is similar, but not identical, to the heating of glass beads by placing them in an external heat bath at a temperature higher than the temperature of the beads. Tseng and Viskanta [7] have found, in modeling the heat flow in glass beads, that the role of radiation transport in determining the thermal history of the material is strongly dependent on the bead size. Thus, it is not possible to generalize the results from these previous studies to other heating situations or other semi-transparent materials.

In particular, when the laser heating is localized, as in laser glass damage mitigation, there is no reason to assume radiation transport plays the same role in determining the overall heat flow in the material as it does in thin rods or beads. In healing a laser glass-damage site, which typically occurs on or near the exit surface of the optic, the idea is to use an infrared laser to heat the material to a temperature above the glass transition temperature (~1600 K) where the viscosity is low, so the material will “flow” and smooth out any surface irregularities, fill in cracks, etc.

The idea of using a low-power far-infrared heating laser for mitigating surface damage to the optical components in a high-power laser system goes back some 30 years [8]. The past work has focused on developing empirically based treatment protocols for mitigating damage sites so the defects or cracks do not grow further on subsequent high-power illumination [9,10]. It has been recognized, however, that the entire thermal history of the damage site --- subsequent cool-down as well as the infrared laser heating phase --- is important in determining the final damage threshold.

On cool-down the structure that “freezes in”, and hence the density of the glass and its residual stress state, is dependent on the cooling rate. The fictive temperature T_f, which is the temperature corresponding to the frozen-in structure of the glass, can be related to the cooling rate q [11]:

$$\frac{d(\ln(q))}{d(\frac{1}{T_f})} = A - \frac{\Delta H}{R}, \tag{1}$$

where A is a constant, ΔH is the activation energy (i.e., the energy required to change the structure from the high-viscosity amorphous “solid” to the low-viscosity amorphous “liquid”), and R is the gas constant. The cooling rate, and hence the fictive temperature, in general varies with spatial position in the material, and hence the thermally cycled glass will have different optical and mechanical properties at different positions.

Since the optical and mechanical properties of glass are strongly dependent on temperature history, in modeling the temperature history one must take proper account of all material properties that are temperature dependent. Not only the fictive temperature, but the viscosity, the coefficient of thermal expansion, and the thermal conductivity of the glass are all temperature dependent. In addition, one must take account of all physical processes that transport energy in the glass. Thermal conduction, in which the thermal energy flow is driven by the temperature gradient, is the dominant heat transport mechanism. Electromagnetic radiation, however, is also a temperature-dependent energy transport mechanism. Although the amount of energy in the thermal radiation is negligibly small at these temperatures --- we are considering only temperatures below about 3000 K --- the heated glass radiates predominantly at photon wavelengths to which the glass is largely transparent, as we will see in the next section, so radiation transport may provide a mechanism for heat to escape or to redistribute heat over much longer distances in the glass than does the thermal conduction.

In this paper we report the results of our investigation of the role radiation transport plays in the localized laser-based annealing of silica glass. We begin in Section II with a description of the radiation transport models we used, the laser absorption model, and the temperature-dependent formulations for thermal conductivity, and how all these models were implemented in a 2D radiation-hydrodynamics computer code. We then discuss the results of the 2D and 1D modeling in Section III. Discussion and summary are presented in Section IV.

II. The Model

The radiation field is described by the radiant energy in the spectral interval $d\nu$, passing per unit time through a unit area, and propagating within an elemental solid angle interval $d\mathbf{\Omega}$ about direction $\mathbf{\Omega}$,

$$I_\nu(\mathbf{r},t,\mathbf{\Omega})d\nu d\mathbf{\Omega}. \tag{2}$$

Following the customary notation, the subscript ν denotes that the variable is spectrally dependent; the total radiant energy $I(\mathbf{r},t,\mathbf{\Omega})$ is, of course, the integral of $I_\nu(\mathbf{r},t,\mathbf{\Omega})$ over ν. The spectral intensity I_ν is obtained by solving the radiation transport equation:

$$\frac{1}{c}\left(\frac{\partial I_\nu}{\partial t}+c\Omega\bullet\nabla I_\nu\right)=\alpha_\nu(B_\nu-I_\nu). \tag{3}$$

Here α_ν is the spectrally dependent absorption coefficient and B_ν is the Planck intensity --- independent of $\mathbf{\Omega}$ --- at photon frequency ν. Eq. 3, of course, describes radiation transport in a non-refractive medium, and assumes that every point in the material is in local thermodynamic equilibrium, a reasonable assumption for heated solids and liquids.

In general, the radiation transport equation can be solved only numerically. In practice, there are several approximations that can yield analytic solutions. In the diffusion approximation, the spectral flux is nearly isotropic, so the net flux, which is the integral of the spectral intensity over all directions, is approximately zero. In applying this approximation to equation 3, it is relatively straight-forward to show that the spectral flux can be approximated by:

$$S_\nu = \frac{c\lambda_\nu}{3}\nabla U_\nu \tag{4}$$

where

$$U_\nu = \frac{1}{c}\int_{4\pi} I_\nu d\Omega$$

is the spectral energy density, dependent on temperature, and λ_ν, the mean free path for photons of frequency ν, is $\lambda_\nu = 1/\alpha_\nu$.

The diffusion approximation is valid only where the photon mean free path is small compared to the gradient scale length over which the temperature changes appreciably. It is not at all clear that the diffusion approximation will be sufficiently accurate for fused silica that is heated by a long-wavelength laser, for which the absorption depth is small, while the material is largely transparent to the higher-energy photons emitted by the heated material. It is possible to obtain a more accurate solution to the radiation transport equation via the P_n approximation. In this approximation, the spectral intensity is written as a series of Legendre polynomials in 1D [12]. This approximation is equivalent to discretizing the photon directions as spherical harmonics in azimuthally symmetric geometries, where Ω depends only on the polar angle. The more harmonics one includes in the series (i.e., the more Legendre coefficients in the series), the more accurate the solution.

In this study, we compare multi-group diffusion (MGD) with P_n as applied to the heating and cooling of fused silica. Grey diffusion (the diffusion approximation with a single value of the absorption coefficient for all photon energies) is inadequate because the silica absorption varies widely with photon energy, as shown in Fig. 1. The spectral absorption coefficients shown in Fig. 1 were pieced together from various sources [13,14,15,16]. In this composite absorption coefficient, the transparent optical band is evident. Note that in the photon energy band corresponding to the peak of the thermal (Planckian) emission at temperatures between ~300 K and ~3000 K, the absorption coefficient varies over nearly seven orders of magnitude.

Our model does not account for the effects of refraction, or the wavelength dependence of the index of refraction. Refraction leads to a variable propagation direction for the photon, so the radiation transport is modified. Castor shows [17] that refraction modifies both the Planck intensity and the absorption because of the interaction of the propagating electromagnetic wave with the induced electric dipole moment in the material. He shows that the right-hand side of equation 3 is modified by replacing α_ν by α_ν/n^2, with n the index of refraction, which itself is dependent on photon frequency. Kitamura *et al.* show [16] that, for fused silica glass, the index of refraction is approximately constant (n~1.5) between about 0.15 μm and 7 μm wavelength; at ~9.2 μm wavelength n spikes up to 3-4, just in the wavelength range where, according to Kitamura *et al.*, there is considerable variation in the measured n's reported by various investigators. The Kitamura *et al.* absorption coefficients at ~9-11 μm are about an order of magnitude less than the absorption coefficients reported by some previous investigators at these longer wavelengths. Assuming their reported values are the more accurate ones, we adopted the Kitamura *et al.* absorption coefficients in constructing the composite absorption coefficients shown in Fig. 1 for photon wavelengths longer than 6.2 μm (0.20 eV) as a partial "mock up" for the effects of the variable index of refraction of the silica. We note that Shestakov *et al.* [18] have recently developed a computational MGD scheme that includes refraction --- as well as reflective boundary conditions --- and incorporated the new scheme in a finite elements solid mechanics code. Future research will make use of the new computational capability to explore the effects of refraction for this particular problem.

The absorption coefficients shown in Fig. 1 were defined in 565 photon energy groups and input into the 2D radiation-hydrodynamics code Lasnex [19], which has routines for both MGD and P_n radiation transport. The ostensibly more-accurate P_n, however, works only in 1D. Thus, in order to do both affordable and accurate MGD in 2D, we first compared MGD with P_n in 1D while varying the number of groups in the MGD simulations spanning the entire photon energy range, starting with the 565 groups we described above. The absorption coefficients for each group in the runs with a smaller total number of groups were calculated as the harmonic mean of the composite opacities over that group. In this manner we determined that a judicious selection of 14 groups, listed in Table I, provides results little different from the results obtained in a 565-group P_n simulation with 31 Legendre coefficients. We then used these fourteen-group absorption coefficients in all the subsequent 2D simulations. We note that the MGD results begin to differ significantly from the P_n results when using fewer than 10 photon energy groups. Thus, as we suspected at the start, grey diffusion is totally inadequate.

Since Lasnex is a plasma code (i.e., it has separate temperatures for electrons and ions), we had to modify the code to be able to treat the material as having a single material temperature. Accordingly, we tie the electrons and ions together by putting a huge multiplier on the electron-ion collision cross section that is hard-wired into the code, and add our own custom routine to calculate the temperature-dependent thermal conductivity, bypassing the separate hard-wired plasma conductivity routines for electrons and ions:

$$k_c(\mathrm{W/m\text{-}K}) = 1.5+0.000667[T(\mathrm{K})-373]. \tag{5}$$

Equation 5 was constructed from the data presented by Kunc *et al.* [14].

The problem we address is the localized heating and cooling of a pure silica slab that is 10 mm thick and 25 mm in diameter. Both the axial and the radial zoning is feathered (zone thickness varied), so that the largest zone thickness axially is in the middle of the slab, and the smallest at the heated end. Since the absorption depth of the 10.6-μm heating laser varies with temperature between ~50 μm and ~3 μm, as discussed in more detail below, the smallest zone at the surface has an axial thickness of 0.1 μm for sufficient resolution of the heated region. The zone thickness in the radial direction depends on the laser spot size, which for our application is always small compared to the slab diameter, so that the heating is localized. For a spot size of 1 mm diameter, the zone thickness in the radial direction at the center of the spot is 70 μm. For 1D simulations, we use a single small-radius zone in the radial direction, and in order to get the incident beam intensity correct, we scale the incident power by the ratio of the 1D zone area to the actual beam area.

The radiation boundary conditions are defined by placing the slab in an external 300 K radiation "bath", the so-called Milne boundary condition. We suppress conduction across the boundaries by setting conductivity to zero at the boundaries, and we do not account for internal reflection at the boundaries.

Heating of the slab is by absorption of a 10.6-μm (0.117 eV) laser beam. We do account for the 15% of the laser energy that is reflected at the surface, so that the total power absorbed is $P_A = 0.85P_0$, where P_0 is the incident laser power. The absorbed laser beam power P_A is put directly into the material internal specific energy exponentially with depth z into the slab; i.e.,

$$p_z = (P_A / m_z)\exp[\int_0^z (-\alpha(T)dz)]. \tag{6}$$

Here, p_z is the specific energy deposition rate into the zone at depth z and mass m_z. The temperature-dependent absorption coefficient for the 10.6-μm laser light is constructed from the data presented by McLaclan and Meyer [13]:

$$\alpha(\mu m^{-1})=(4\pi/10.6)\{0.0182+0.0001[T(K)-273]\}. \tag{7}$$

The deposition profiles at four separate times for 2.35 W incident laser power on for 10 s in a 1D simulation are shown in Fig. 2. As is clear from this figure, at the start of the laser pulse, when the material is still cold, most of the energy is deposited in a region near the surface that has an e-folding depth of some 50 μm, consistent with equation 7. As the material heats, the deposition depth shrinks. At T=3000 K it is only about 3 μm deep.

We also did simulations with heating of the silica slab by absorption of a 4.6-μm (0.270 eV) laser beam. The absorption coefficient for 4.6 μm light is much less than that for 10.6 μm light, as seen in Fig. 1, so the absorption depth is much greater:

$$\alpha(\mu m^{-1})=(4\pi/4.6)\{0.0305+0.0000894[T(K)-273]\}x10^{-2}. \qquad (8)$$

The shorter-wavelength laser thus provides deeper and more uniform heating in the surface layer for healing of buried damage sites. Note that the 4.6 μm laser absorption is, as for the 10.6 μm photons, linear with temperature, with eq. 8 constructed from recent data of Yang [20]. Note also that we account for the temperature dependence of the absorption coefficients only for the deposited photons; the radiation transport calculations are done with the "cold" absorption coefficients shown in Fig.1 at all temperatures. Very little data exist on the temperature dependence of absorption coefficients in silica over the full range of photon wavelengths.

The time step in the simulations must be kept smaller than the thermal diffusion time across the heat deposition depth, $(\rho C/k_c)(1/\alpha^2) \sim 1$ ms, where C=0.7 J/(gm-K) is the material specific heat, ρ=2.21 g cm^{-3} is the silica density, k_c is the thermal conductivity given by equation 5, and α is the absorption coefficient given by equation 7. When simultaneously accounting for energy deposition, thermal conduction, and radiation transport, operator-split errors accumulate (i.e., errors arise from the fact that the different equations are solved in a certain order of succession) if the time step is not actively constrained from growing too large. The constraints on zone size, time step, and number of photon energy groups mean that accurate 2D simulations are costly.

We ignore convective losses at the boundary, and also ignore evaporation, which is negligible at temperatures below about 2800 K [21]. Since both convection and evaporation cool the material, and the radiation losses are less at lower temperature, neglect of convective and evaporative losses in our modeling provides us with an upper limit to the relative amount of radiation cooling.

III. Results

The maximum temperature occurs at the center of the laser spot on the surface at the time the laser turns off, and then the surface cools rapidly as the heat transports in, out, and laterally. A 2D pseudo-color temperature contour plot for a simulation in which 6 W of 10.6-μm laser radiation is incident on the silica slab for 5 s in a 1-mm-diameter spot is shown in Fig. 3.

The value of the maximum temperature depends on the laser power, as shown in Fig. 4. Here, we show maximum temperatures reached for 4.6-μm and 10.6-μm laser illumination. As discussed above, silica is less opaque to 4.6-μm photons (eq. 8) than it is to 10.6-μm photons (eq. 7), so the heating is spread over a larger absorption depth in the material. Hence, it takes more laser power at 4.6 μm laser wavelength to heat to the same peak temperature to which the 10.6 μm laser heats.

Once the laser turns on, the temperature in the center of the spot at the surface rises rapidly, and then tends to level off as a steady state is approached, as shown in Fig. 5. Here we show the simulated temperature history in the center of the spot at the surface with and without radiation transport for 9 W of 10.6-μm laser radiation in a 1-mm-diameter spot on for 5 s. At 5 s, as soon as the laser turns off, the heated spot cools rapidly, at a rate of more than 6500 K/s at spot center. With radiation cooling, the peak temperature is only ~1% cooler, and the cooling rate at laser turn-off is only slightly less --- 30 K/s less --- than it is for conductive cooling alone. Thus, radiation transport tends to cool the hot spot, as expected, but only slightly faster than cooling provided by thermal conduction alone.

Now let us look more closely at the distribution of heat at one particular time, 5 s. Over the five seconds the material is being heated in a 1-mm spot on the surface, heat is transported both axially and radially into the surrounding cold material. In Fig. 6 we show the radial temperature profile at 5 s and in Fig. 7 the axial temperature profile at 5 s from the same 2D simulation as in Fig. 5. The radiation transport slightly heats a region of the material outside the heated spot more than the heating provided by the thermal conduction alone, as shown in Fig. 8 in the radial temperature difference profile (temperature with radiation transport minus temperature without) at 5 s. This extra heating by the radiation is very slight, amounting to less than 1 K approximately 3 mm out from the center of the ½-mm-radius spot in the 12 W case, for which the peak temperature is nearly 3000 K. In the axial direction there is no extra heating provided by the radiation, as seen in the axial temperature difference profile at 5 s in Fig. 9.

Likewise, radiation transport makes little difference to the cooling rates. Fig. 10 shows the radial cooling rate difference profiles (the cooling rates between 5.0 s and 5.2 s, as the peak temperature drops below the glass transition temperature) and Fig. 11 the axial cooling rate difference profiles for the same laser powers as in Fig. 8 and Fig. 9. Even at an incident power of 12 W, the cooling rate is only about 0.5% slower with radiation than without near the center of the spot, and only slightly faster about 3 mm radially out from the center. From equation 1 and the data presented in Ref. 11, this result implies that radiation transport accounts for an additional change in the fictive temperature by less than 1 K. The dominant conductive cooling, on the other hand, has a significant effect on the fictive temperature profile in the material, confirmed in recent measurements by Matthews *et al.* [22].

The problem we are considering here, where the laser beam spot is much smaller than the diameter of the slab being heated by the laser, provides a lower limit to the effects of radiation cooling. This is because the heat in the hot spot can conduct radially as well as axially into surrounding colder material. When the beam spot completely fills the diameter of the glass we should expect a much larger relative effect of radiation cooling, because there is much less conductive cooling in the radial direction. To estimate the relative effect of radiation in the case where the beam spot fills the entire surface, we also performed these simulations in 1D, using P_n radiation transport and the full 565 photon energy groups. The 1D simulations had symmetry boundary conditions on the radial edges (as if the slab has infinite diameter), so we are not accounting for radiation losses at the edges. Thus, the 1D simulations do not provide an exact upper limit to the relative effect of radiation cooling out the surface, but they will provide a reasonably good estimate. For the 2D case, we see in Fig. 4 that a laser power of approximately 10.5 W in a 1-mm-diameter spot is required to heat the silica to a peak temperature of about 2600 K in 5 s, and we have shown (Fig. 5) that approximately 1% of the energy is radiated away by the time of laser turn-off at 5 s. In 1D, a laser power of only 2.35 W in a 1-mm-diameter spot gives about the same peak temperature, and here we find an approximate 5% radiation energy loss out the heated surface at the time of laser turn-off.

Even in this 1D case, then, the conductive flux, $k_c dT/dz$, dominates the heat transport where the temperature gradients are high, as shown in Fig. 12. In this simulation, the total flux deposited by the laser is 2.55 W/mm^2 [i.e., 2.35 W x 0.85/(π x 0.5^2 mm^2)]; all but the approximately 5% of it that is radiated away is transported into the surrounding cold material by conduction. As seen in Fig. 12, the heat conduction wave moves into the silica ~3 mm in the 5 s the laser is on, consistent with an analytical estimate from the heat conduction equation.

What is unique about the radiation transport, however, in transporting heat in the material is that a not-insignificant fraction of the radiation energy density is in photons with much longer radiation mean free paths than the infrared photons that deposit the energy. In Fig. 13 we show profiles at 5 s and 10s of the spectral intensity I_n integrated over the nine spectral bands shown in Fig. 13a. Note that the energy is deposited into the material in band 3, which contains the 10.6 μm laser photons, but a large fraction of the radiation energy in the material is redistributed into band 4. The photons in band 4 have a mean free path ~0.5 mm, nearly two orders of magnitude greater than do the photons in band 3. Thus, the small fraction of the deposited energy that goes into the radiation field can be transported more quickly over larger distances in the material than the energy transported by heat conduction. Most of this radiation energy is radiated out the front (heated) surface, with a small fraction transported to the back of the slab, as shown in Fig. 14. Here we show the profiles at 5 s and 10 s of the spectral flux in these same nine spectral bands. We compute the spectral flux as $(1/3\alpha_n)dI_n/dz$ (per eq. 4), where the subscript n refers to the quantity in the photon energy band n. The flux near the surface is predominantly out the surface and is limited by the free-streaming value, $(c/3)U_n$. Note that most of the radiation flux is in band 4 because this is the band that contains most of the radiation energy with long mean free paths. The radiation flux profile is already several mm wide by 5 s, and by 10 s there is already a very small amount of radiation escaping out the back surface, even before the heat diffusion wave gets there.

IV. Discussion and Summary

The problem we are considering is quite different than the problem considered by Larsen [23, 24] and the general problem of the cooling of glass molds. In these latter cases the entire volume of the slab is heated to some high temperature, and thus the temperature gradient is initially zero everywhere and cooling is dominated by radiation transport out the surfaces. In these cases, heat is being drawn out of the bulk from depths comparable to the mean free path of the photons that carry the bulk of the radiation energy, so the temperature history at and near the surface is very different with and without radiation transport. In those cases, it is important to include the radiation transport in modeling the cooling. In our case, however, where only a relatively thin surface layer of the glass is brought to some high temperature by the heating laser, a heated layer which is much thinner than the radiation mean free path, there is very little heat at depths of a mean free path from which the radiation transport can draw. Thus, the role of radiation transport in the cooling of the glass is much less, and, in fact, can be largely neglected if one is content with estimating the temperature history only to within about 1%-2%.

There is, however, a very important caveat attached to this conclusion. We computed radiation transport using “cold” absorption coefficients. We included a formulation for the temperature dependence of the absorption coefficient only for the heating photons, photons of 10.6 μm or 4.6 μm wavelength, and then only in computing the laser deposition. There is a dearth of data on the temperature dependence of the absorption coefficient of silica over the entire wavelength range of interest here. We would expect, however, that the absorption coefficient will increase with temperature for all photon energies, so the effect of accounting for this temperature dependence would be to increase the radiation cooling, since the mean free path of the photons carrying the bulk of the radiation energy will decrease as the temperature increases and hence move in the direction of becoming more comparable to the depth of the heated layer. This is a topic for further research, but our very preliminary estimates suggest that accounting for temperature dependence of the absorption coefficients can add another 1-2% of the deposited energy radiated away during the time the laser is on.

Can a ~4% effect be important in determining mechanical properties such as the final stress states in the material and the final surface distortions? This is difficult to say, since the final stress states and surface profile depend on the temperature-dependent viscosities and thermal expansion coefficients, quantities that are not known to much better than a few percent. Furthermore, the estimated 4% effect of radiation cooling on the peak temperatures is only for peak temperatures well above 2000 K (the effect of radiation cooling is much less at lower temperatures), and at these higher temperatures evaporative cooling begins to play a role [20]. The vapor phase of silica may (and probably does) contain different molecules than the solid phase as the SiO_2 molecules dissociate and recombine in different ways. How does the radiation from the surface interact with the time-varying chemistry of the vapor? How does the radiation change the chemistry? How does the vapor change the amount of energy deposited by the incoming laser? What role does radiation transport play in the presence of evaporation? These are all open questions.

In summary, we have formulated a computational model for the heating and cooling of silica, and have incorporated this model into a 2D radiation-hydrodynamics computer code. We find that, in 1D, for about 2.35 W of incident illumination over 5 s in a 1 mm spot with 10.6 μm laser light, about 5% of the deposited energy radiates out by the time of laser turn-off. In 2D, about 10 W of illumination is required to bring the peak temperature of the silica to approximately the same value in 5 s in a 1 mm spot as in the 2-W 1D case, and then only about 1% of the deposited energy radiates out by the time of laser turn-off. Most of the radiated energy is in higher-energy photons than the infrared photons that deposit the energy, and these photons have a mean free path in the material nearly two orders of magnitude greater than the absorption depth. Thus, the effect of radiation transport is to flatten the temperature gradient but steepen the fictive temperature gradient, but only by a very small amount. Thus, radiation transport plays only a very small role in the localized infrared laser heating and cooling of silica, but it may play a role in other processes that determine the final states, including evaporative cooling and the chemical dynamics of the vapor.

Acknowledgments

The authors acknowledge useful and enlightening discussions on all aspects of this work with Jeff Bude, Manyalibo Matthews, and Michael Feit of the Lawrence Livermore National Laboratory. Matthews and Feit provided a critical reading of early drafts of this paper which the authors believe have substantially improved the final product. Help in adapting the Lasnex code to handle this particular problem was provided by John Castor and Judy Harte of Lawrence Livermore National Laboratory. This work was performed under the auspices of the US Department of Energy by Lawrence Livermore National Laboratory under contract No. DE-AC52-07NA27344, with support received from LDRD Project #08-ERD-057.

References

[1] C. W. Ponader, J. M. Schroeder, and A. M. Streltsov, “Origin of the refractive-index increase in laser-written waveguides in glasses”, *J. Appl. Phys.* **103**, 063516 (2008).

[2] T. D. Bennett and L. Li, “Modeling laser texturing of silicate glass”, *J. Appl. Phys.* **89**, 942-950 (2001).

[3] K. M. Nowak, H. J. Baker, and D. R. Hall, “Efficient laser polishing of silica micro-optic components”, *Appl. Optics* **45**, 162-171 (2006).

[4] G. M. Homsy and K. Walker, “Heat transfer in laser drawing of optical fibres”, *Glass Technology* **20**, 20-26 (1979).

[5] W. Tian and W. K. S. Chiu, “Temperature prediction for CO_2 laser heating of moving glass rods”, *Optics and Laser Tech.* **36**, 131-137 (2004).

[6] W. Tian and W. K. S. Chiu, “Radiation modeling of stationary fused silica rods and fibers heated by CO_2 laser irradiation”, *Numerical Heat Transfer Part A* **46**, 115-130 (2004).

[7] C. C. Tseng and K. Viskanta, "Heating/melting of fused silica by convection and radiation", *Int. J. Heat Mass Transfer* **49**, 2995-3003 (2006).

[8] P. A. Temple, W. H. Lowdermilk, and D. Milam, "Carbon dioxide laser polishing of fused silica surfaces for increased laser damage resistance at 1064 nm", *Appl. Optics* **21**, 3249-3255 (1982).

[9] R. M. Brusasco, B. M. Penetrante, J. A. Butler, S. M. Maricle, and J. E. Peterson, "CO_2-Laser Polishing for Reduction of 351-nm Surface Damage Initiation in Fused Silica", in *Proc. SPIE* **Vol. 4679**, 34-39 (2002).

[10] P. Bouchut, L. Delrive, D. Decruppe, and P. Garrec, "Localized silica re-fusion for laser damage mitigation", in *Proc. SPIE* **Vol. 5273**, 250-257 (2004).

[11] D. L. Kim and M. Tomozawa, "Fictive temperature of silica glass optical fibers – re-examination", *J. Non-Cryst. Solids* **286**, 132-138 (2001).

[12] G. C. Pomraning, *The Equations of Radiation Hydrodynamics* (Dover Pub., Inc., Mineola, N. Y., 2005).

[13] A. D. McLaclan and F. P. Meyer, "Temperature dependence of the extinction coefficient of fused silica for CO_2 laser wavelengths", *Appl. Optics* **26**, 1728-1731 (1987).

[14] T. Kunc, M. Lallemand, J. B. Saulnier, "Some new developments on coupled radiative-conductive heat transfer in glasses – experiments and modeling", *Int. J. Heat Mass Transfer* **27**, 2307-2319 (1984).

[15] P. G. Nelson, "A Thermal Analysis of a 1.5 Meter f/5 Fused Silica Primary Lens for Solar Telescopes", *Coronal Solar Magnetism Observatory Tech. Note* **13** (2007).

[16] R. Kitamura, L. Pilon, and M. Jonasz, "Optical constants of silica glass from extreme ultraviolet to near infrared at near room temperature", *Appl. Optics* **46**, 8118-8133 (2007).

[17] J. Castor, *Radiation Hydrodynamics* (Cambridge University Press, 2004).

[18] A. I. Shestakov, R. M. Vignes, and J. S. Stölken, "Derivation of multi-frequency radiation diffusion equations for homogeneous refractive lossy media", submitted to *J. Comp. Phys.* (2010).

[19] G. B. Zimmerman and W. L. Kruer, Comments *Plasma Phys. Controlled Fusion* **2**, 51 (1975).

[20] S. T. Yang, Lawrence Livermore National Laboratory, private communication (2009).

[21] S. T. Yang, M. J. Matthews, S. Elhadj, V. G. Draggoo, and S. E. Bisson, “Thermal transport in CO_2 laser irradiated fused silica: In situ measurements and analysis”, *J. Appl. Phys.* **106**, 103106 (2009).

[22] M. J. Matthews, R. M. Vignes, J. D. Cooke, S. Yang, and J. S. Stölken, “Analysis of micro-structural relaxation phenomena in laser-modified fused silica using confocal Raman spectroscopy”, submitted to *Appl. Phys. Lett.* (2010).

[23] E. W. Larsen, G. Thömmes, and A. Klar, “Simplified P_n Approximations to the Equations of Radiative Heat Transfer and Applications”, *J. Comp. Phys.* **183**, 652-675 (2002).

[24] E. W. Larsen, G. Thömmes, and A. Klar, “New Frequency-Averaged Approximations to the Equations of Radiative Heat Transfer”, *SIAM J. Appl. Math.* **64**, 565-582 (2003).

Table I. Photon energy groups used in the 2D simulations. Photon wavelength λ is related to photon energy E_ν by $\lambda = hc/E_\nu$ (i.e., photons of energy E_ν= 1 eV have wavelength λ=1.242 μm).

Group	E_{upper} (eV)	E_{ave} (eV)
1	0.024796	0.014316
2	0.040435	0.031664
3	0.065936	0.051634
4	0.10752	0.084200
5	0.17533	0.13730
6	0.28592	0.22390
7	0.46624	0.36511
8	0.76029	0.59538
9	1.2398	0.97088
10	3.0995	1.9603
11	5.2127	4.0196
12	8.7667	6.7601
13	14.744	11.369
14	24.796	19.120

Figure Captions

Fig. 1. Absorption coefficient of fused silica as a function of photon energy, pieced together from data in References 13-16, as explained in the text. Photon wavelength λ is related to photon energy E_ν by $\lambda=hc/E_\nu$ (i.e., photons of energy $E_\nu= 1$ eV have wavelength $\lambda=1.242$ μm).

Fig. 2. The axial energy deposition profiles at four times for 2.35 W of 10.6-μm laser power incident from the right onto a 10-mm-thick slab of fused silica for 10 s.

Fig. 3. Temperature contours at 5 s from a 2D simulation in which 6 W of 10.6-μm laser radiation is incident from the right on the silica slab for 5 s in a 1-mm-diameter spot. The silica slab is 10 mm thick and 20 mm in diameter. Peak temperature in the center of the spot on the surface is 1796 K.

Fig. 4. Simulated maximum temperature reached in the spot center on the surface as a function of laser power for 10.6 μm (red curve) and 4.6 μm (blue curve) laser irradiation in a 1-mm-diameter spot on for 5 s.

Fig. 5. Simulated temperature history in the center of the spot at the surface with (red curve) and without (blue curve) radiation transport for 9 W of 10.6-μm laser radiation in a 1-mm-diameter spot on for 5 s.

Fig. 6. Simulated radial temperature profile at 5 s for 9 W of 10.6-μm laser radiation in a 1-mm-diameter spot on for 5 s.

Fig. 7. Simulated axial temperature profile at 5 s for 9 W of 10.6-μm laser radiation in a 1-mm-diameter spot on for 5 s.

Fig. 8. Simulated radial temperature difference profiles (temperature profile with radiation transport minus temperature profile without radiation transport) at 5 s for four different powers of 10.6-μm laser radiation in a 1-mm-diameter spot on for 5 s.

Fig. 9. Simulated axial temperature difference profiles (temperature profile with radiation transport minus temperature profile without radiation transport) at 5 s for four different powers of 10.6-μm laser radiation in a 1-mm-diameter spot on for 5 s.

Fig. 10. Simulated radial cooling rate difference profiles (cooling rate profile without radiation transport minus cooling rate profile with radiation transport) at 5 s for four different powers of 10.6-μm laser radiation in a 1-mm-diameter spot on for 5 s.

Fig. 11. Simulated axial cooling rate difference profiles (cooling rate profile without radiation transport minus cooling rate profile with radiation transport) at 5 s for four different powers of 10.6-μm laser radiation in a 1-mm-diameter spot on for 5 s.

Fig. 12. Axial conductive flux profiles at 5 s and 10 s from 1D simulation for 2.35 W of 10.6-μm laser radiation in a 1-mm-diameter spot on for 5 s.

Fig. 13. a) Harmonic average mean free paths for nine photon energy groups spanning the radiation spectrum. b) Axial spectral intensity profiles in the nine photon energy groups at 5 s and c) at 10 s from 1D simulation for 2.35 W of 10.6-μm laser radiation in a 1-mm-diameter spot on for 5 s.

Fig. 14. Axial spectral radiation flux profiles in the nine photon energy groups at 5 s and 10 s from 1D simulation for 2.35 W of 10.6-μm laser radiation in a 1-mm-diameter spot on for 5 s.

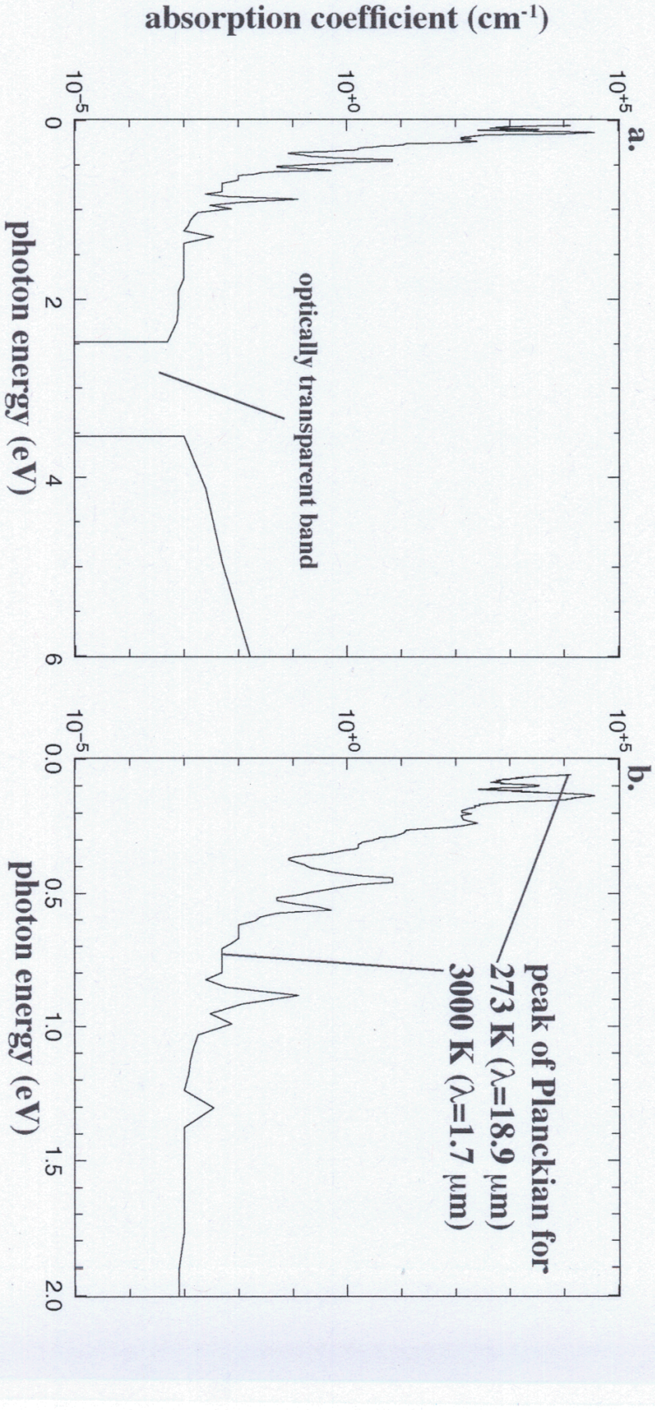

Colvin_Figure_1

Colvin_Figure_2

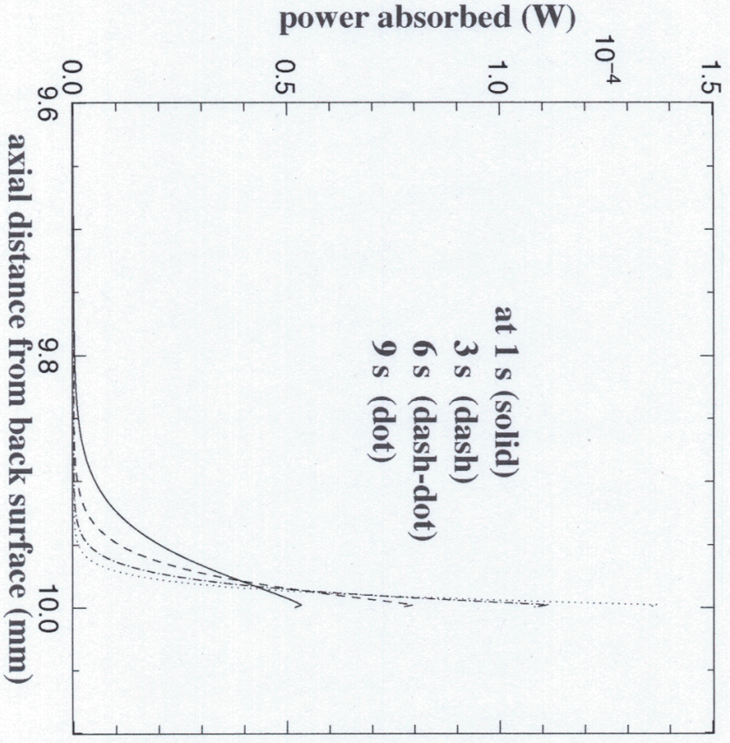

Colvin_Figure_3

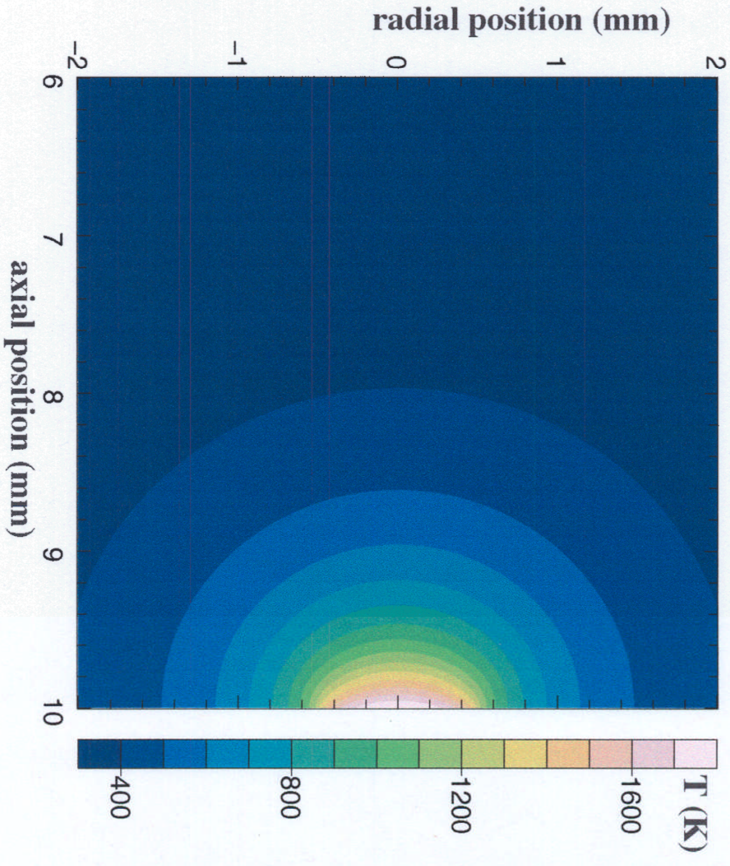

Colvin_Figure_4

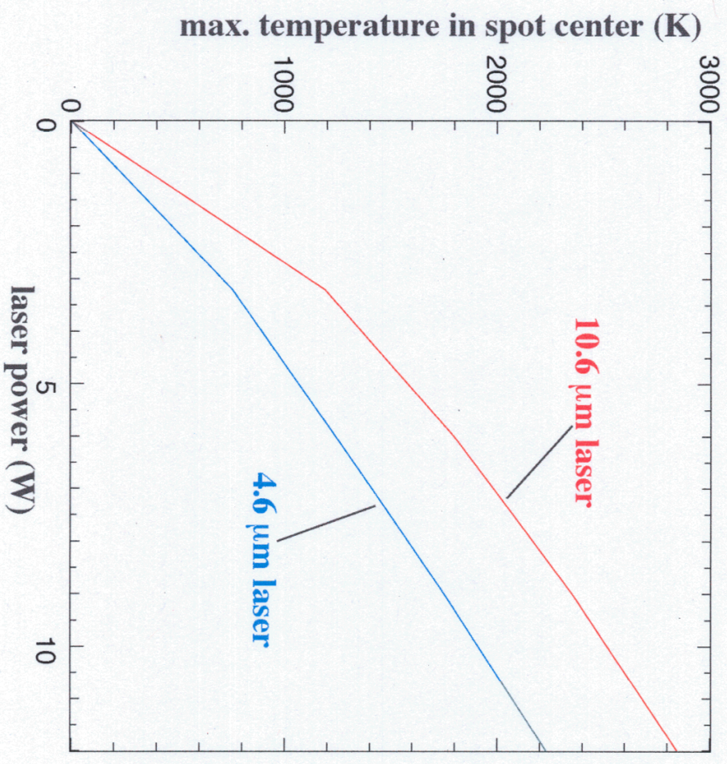

Colvin_Figure_5

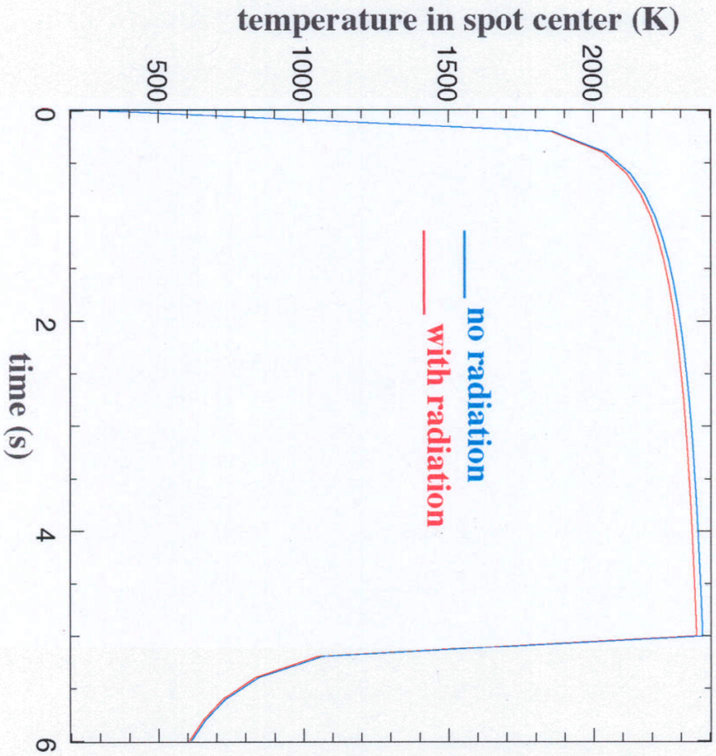

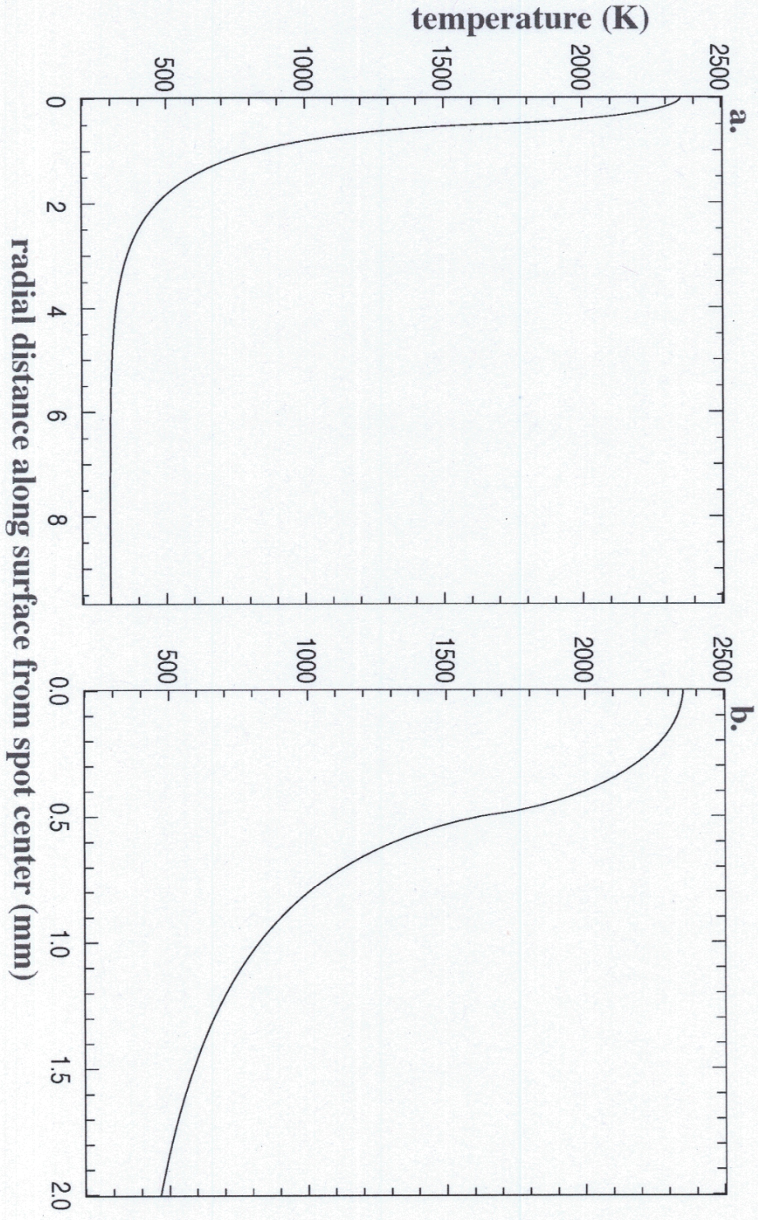

Colvin_Figure_6

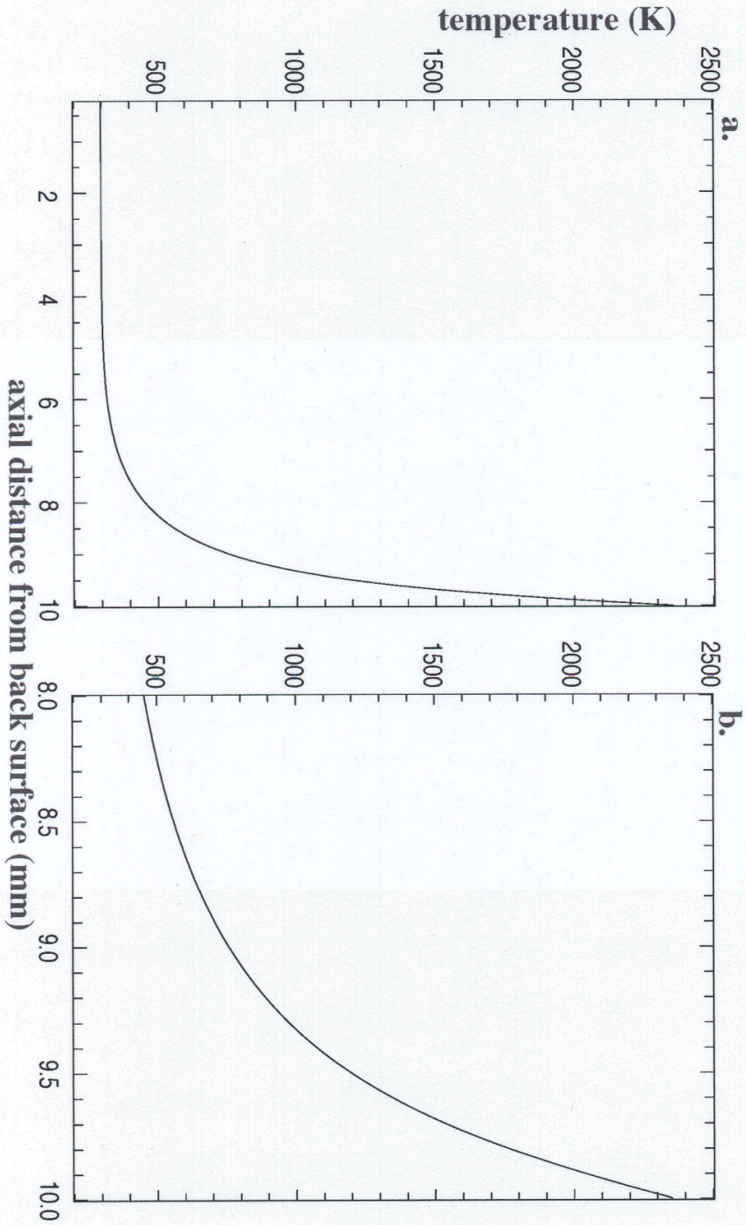

Colvin_Figure_7

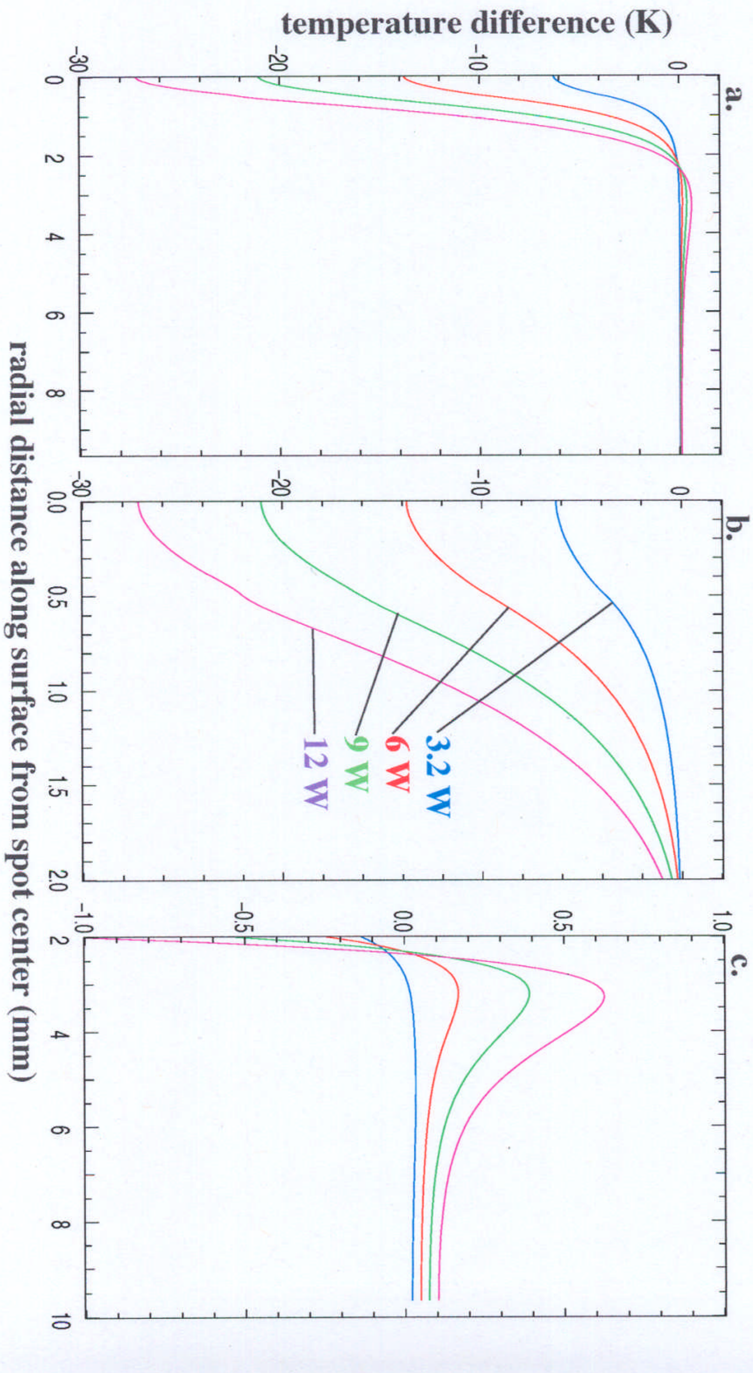

Colvin_Figure_8

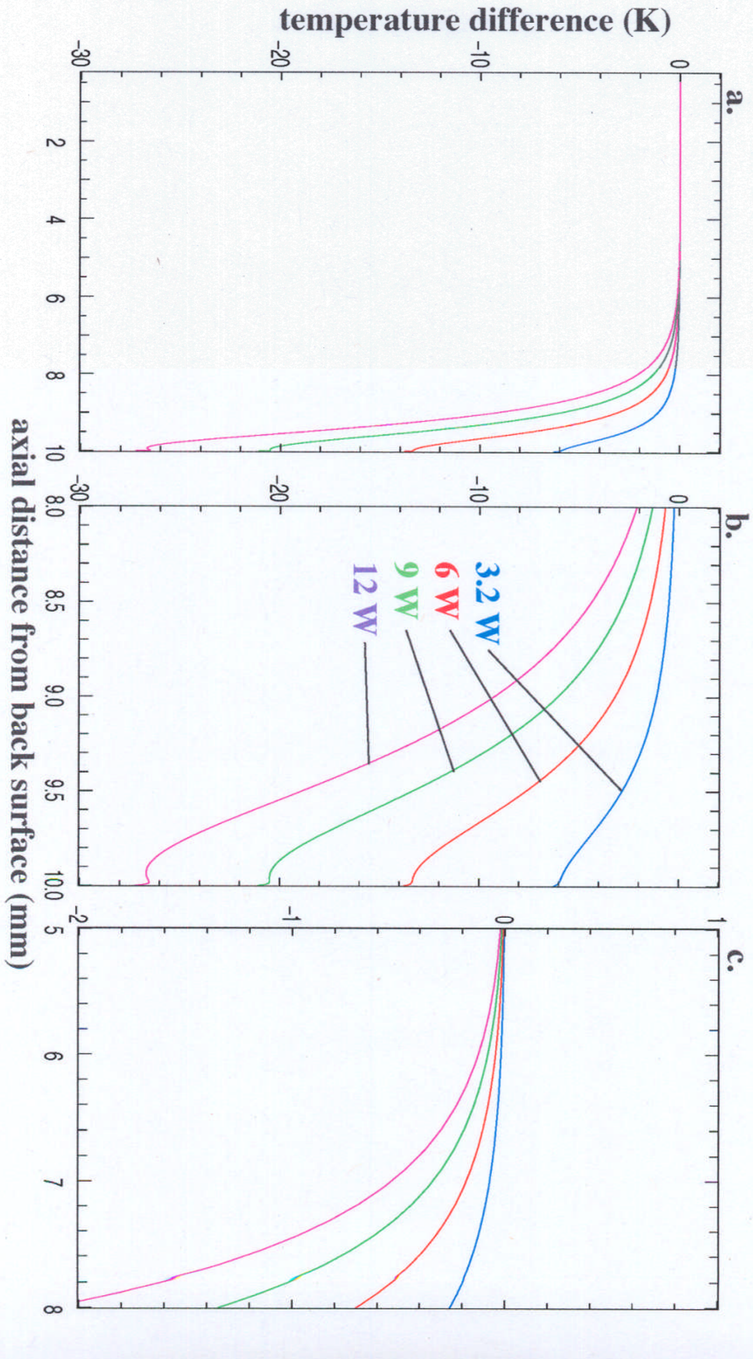

Colvin_Figure_9

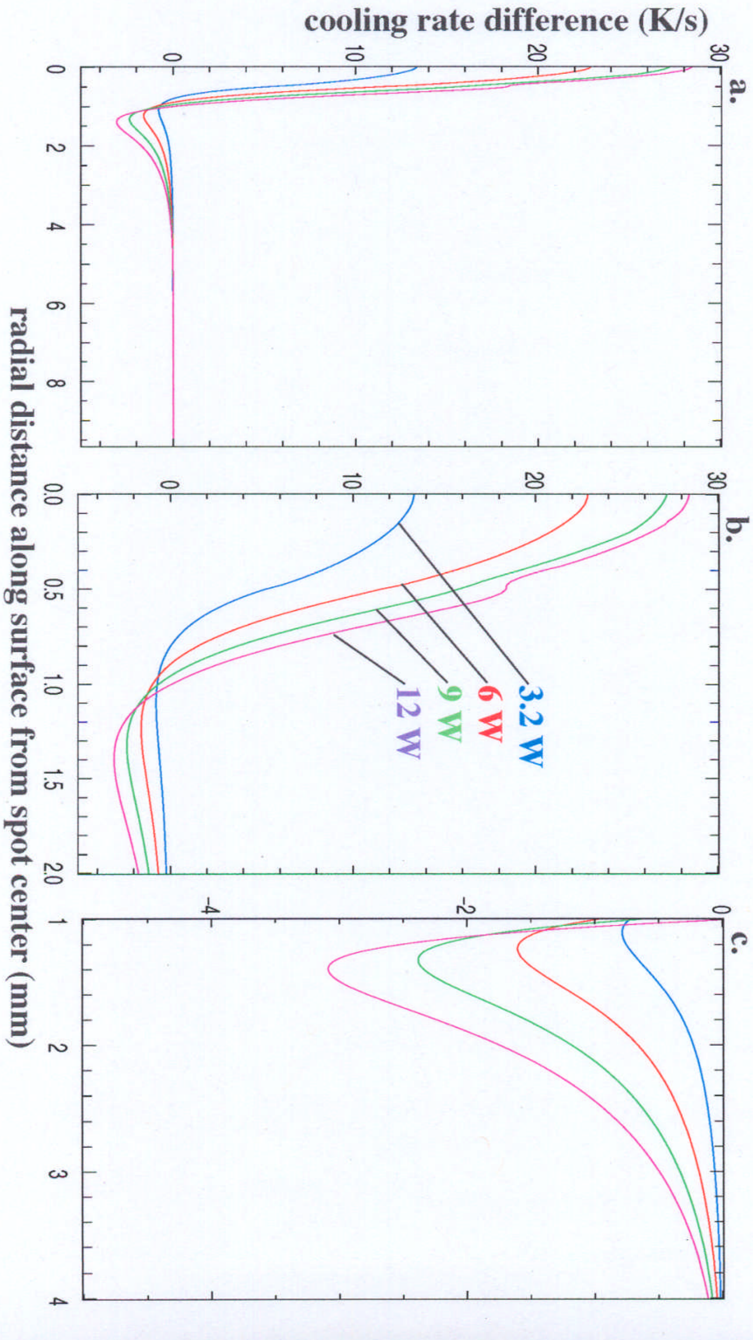

Colvin_Figure_10

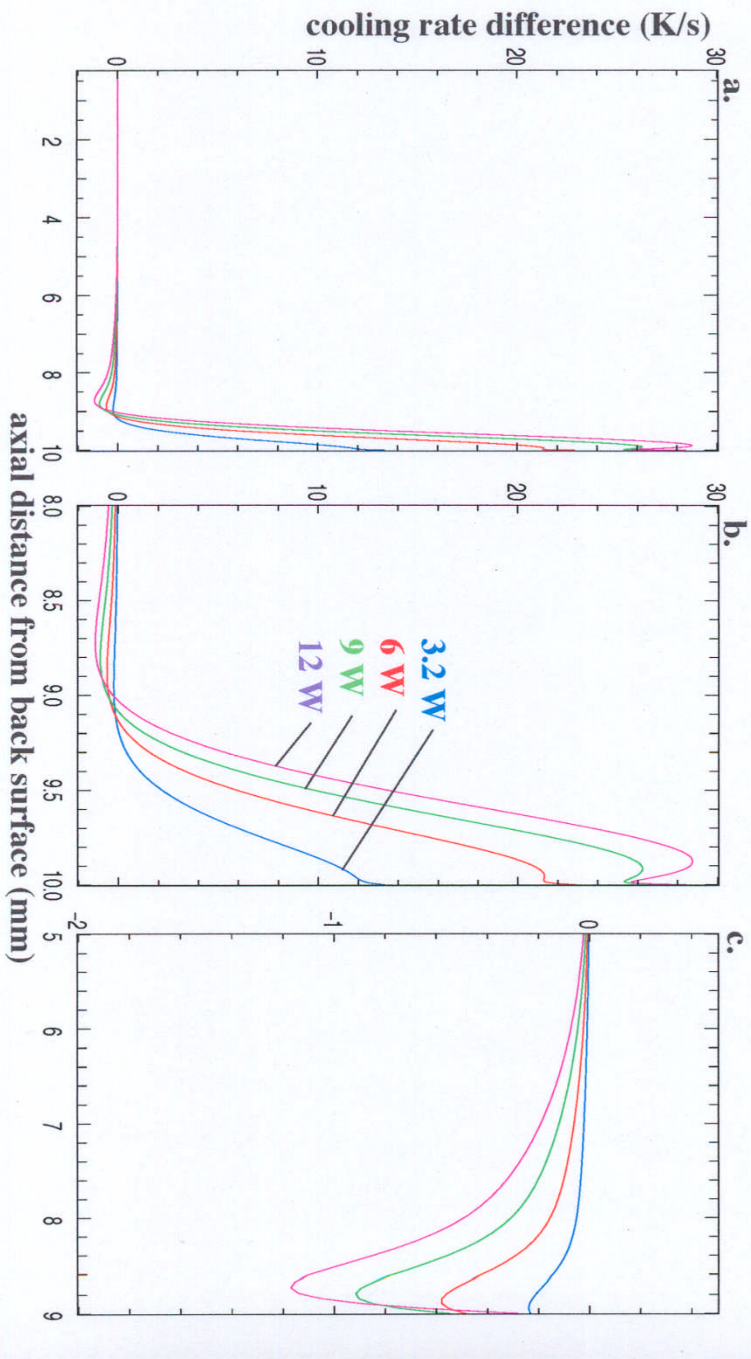

Colvin_Figure_11

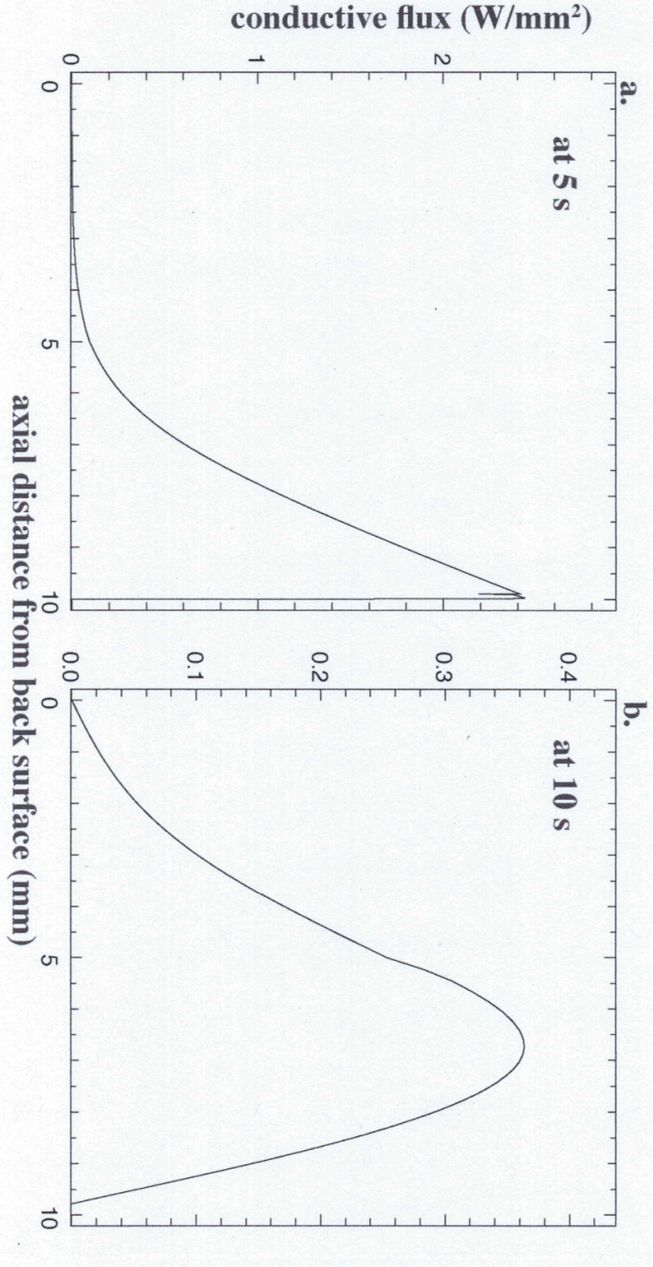

Colvin_Figure_12

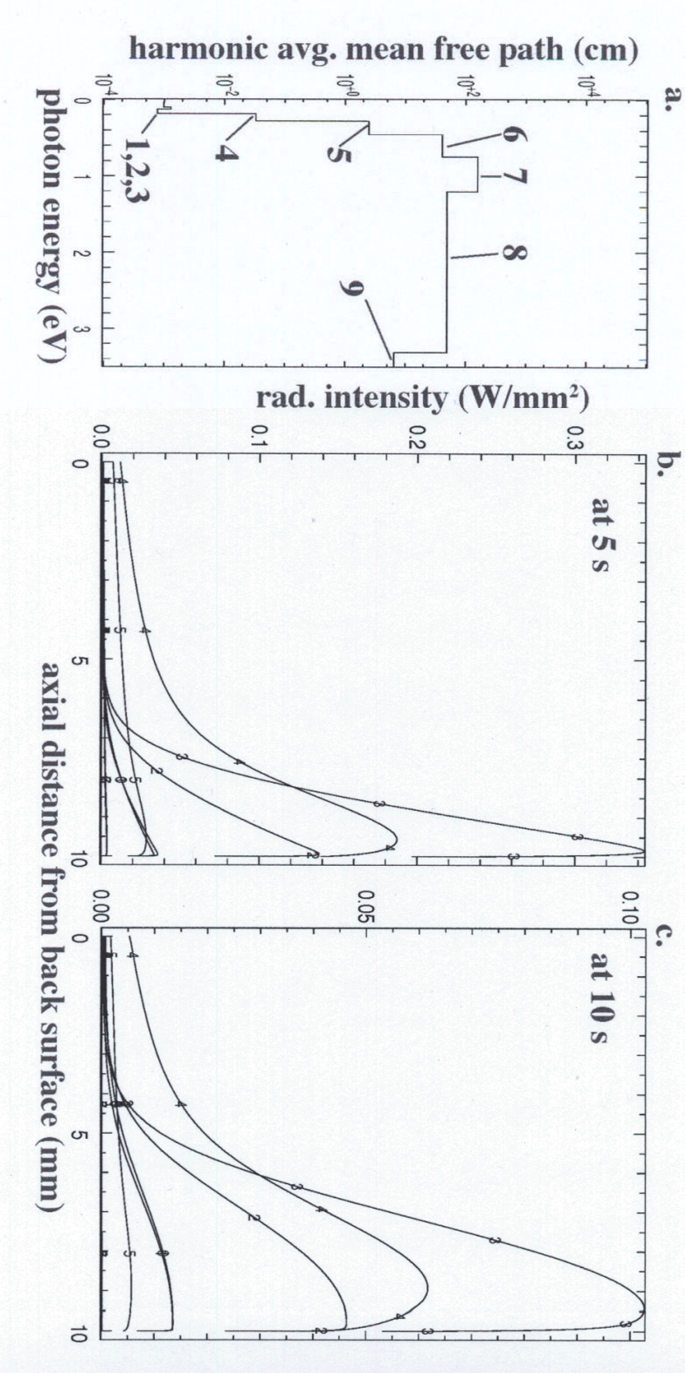

Colvin_Figure_13

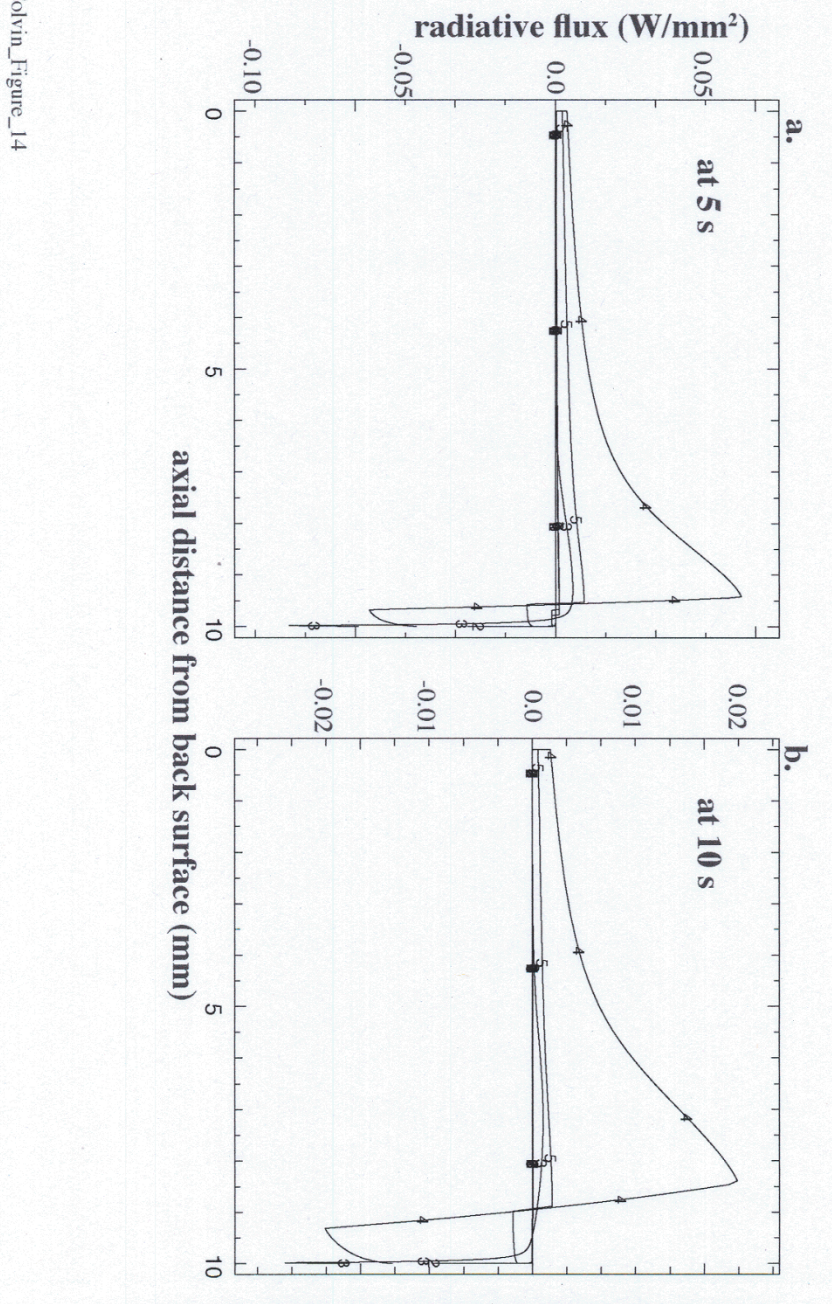
Colvin_Figure_14
radiative flux (W/mm²)
a.
at 5 s
0.05
0.0
-0.05
-0.10
0
5
10
2
3
4
5
b.
at 10 s
0.02
0.01
0.0
-0.01
-0.02
0
5
10
axial distance from back surface (mm)